




A Modification of Adaptive Greedy Algorithm for Solving Problems of Fractured Media Geophysics

Alena V. Favorskaya^{1,2} , Nikolay I. Khokhlov^{1,2} ,
Dmitry A. Podlesnykh¹ 

© The Authors 2024. This paper is published with open access at SuperFri.org

Nowadays, the issue of direct modeling of seismic exploration problems is becoming increasingly important due to the development of a new field of application of such algorithms as generation of a training samples for subsequent solution of the appropriate inverse problem using neural networks. This challenges scientists to develop corresponding parallel algorithms and improve their efficiency. The current manuscript is devoted to the algorithm for decomposing a large number of individual computational grids of various sizes for a large number of MPI processes using the example of a 3D direct problem of seismic exploration of geological media treating the complex topology of the Earth's surface, the complex shape of interfaces between geological layers and a large number of explicitly treated geological fractures, that are not aligned with the coordinate axes. Three modifications of the grid-characteristic numerical method on Chimera and curvilinear computational grids are compared with each other. The dependence on different numbers of fractures is studied. A large number (several hundreds or thousands) of fractures in the geological media significantly increases the amount of transmitted data, which imposes requirements on the developed modification of the greedy algorithm.

Keywords: decomposition, greedy algorithm, large number of grids, large number of fractures, Chimera meshes, patch grids, grid-characteristic method, elastic wave, seismic wave, 3D simulation.

Introduction

Methods for solving inverse problems can be divided into inversion, migration, and the use of neural networks, with each approach imposing its own parallelization features [9, 16]. With the development of neural networks, the issue of direct modeling of seismic exploration problems is becoming increasingly relevant, as a new area of application for this type of computer modeling is actively developing. Training of neural networks for solving inverse problems of wave dynamics on simulated data has been actively carried out in recent years [7, 8, 14, 15]. Another new way of using solvers for direct problems of wave dynamics due to the development of neural networks is the use of deep learning to obtain seismograms from a velocity model [22], which also creates a need to use synthetic training samples. This means that the development of new high-precision methods for three-dimensional modeling of seismic waves in geological media, treating the complex surface topography and internal structure, with explicit identification of fractures, that are not co-directed with the coordinate axes, is acquiring additional significance and relevance. In turn, the question arises of the quality of parallelization of the developed algorithms and taking into account the efficiency of parallelization as a factor in choosing the best method of computer modeling.

In recent years, the following numerical methods for solving direct problems of seismic exploration, the development of which is underway, have become popular, i.e., finite-difference method on staggered grids [21], the discontinuous Galerkin method [20, 24], and the spectral element method [23].

¹Moscow Institute of Physics and Technology, Dolgoprudny, Russian Federation

²Scientific Research Institute for System Analysis of the National Research Centre "Kurchatov Institute", Moscow, Russian Federation

The following two main types of accounting for fracturing in geological environments are distinguished, i.e., explicit treatment of fractures [4, 6, 10] and different averaged models [4, 17].

The paper [24] is devoted to parallelized modification of the discontinuous Galerkin method for solving geophysical problems, but a large number of individual computational grids does not arise. The paper [1] considers the issue of decomposition of structured and unstructured grids when solving problems of linear elasticity and using fine and coarse grids with different integration steps. The papers [11, 18] are devoted to the decomposition of methods using overlapping patch grids, which are used to increase the number of nodes in the desired area.

In this manuscript, we compare three modifications of the grid-characteristic method in terms of their parallelization efficiency, i.e., the grid-characteristic method on curvilinear structured grids [5] (type #1), the grid-characteristic method on Chimera grids for describing the topography of the Earth's surface and interfaces between geological rocks [2], which we combine with two methods for treatment fracturing, i.e., the use of Chimera rotated Cartesian grids around fractures [12] (type #2) and the use of overlapping patch grids around fractures [13] (type #3). The novelty of this study is that we consider a different large numbers of fractures and a larger number of MPI processes.

The article is organized as follows. Section 1 is devoted to problem statement and mathematical model. In section 2 we introduce decomposition and partitioning algorithms. Section 3 contains speed up testing. Conclusion summarizes the study and points directions for further work.

1. Problem Statement and Mathematical Model

To describe the propagation of seismic waves in geological media with complex boundaries (see Fig. 1) and multiple fractures (see Figs. 2–4), we seek a solution to the following initial boundary value problem of the hyperbolic elastic wave equation.

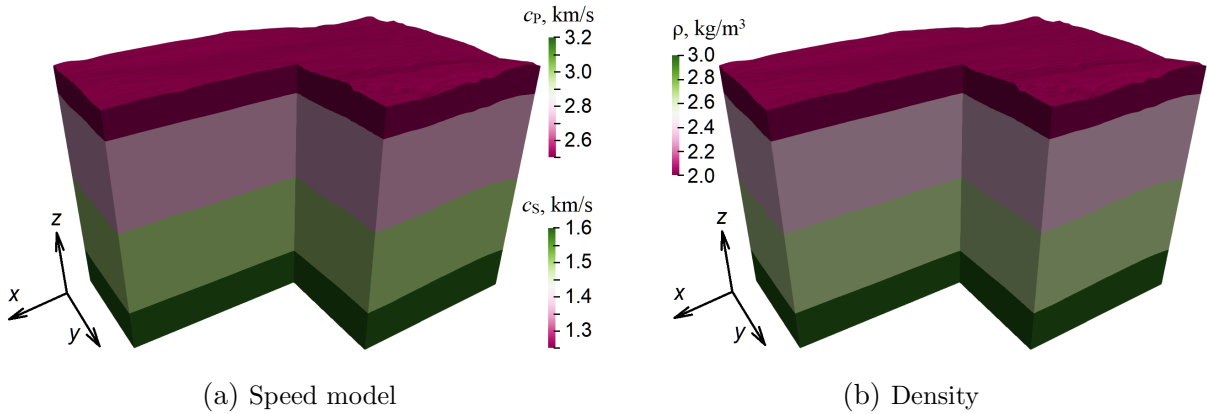


Figure 1. Geological model with 4 layers

The system of equations inside the integration domain in each geological layer $\#l$ is written as follows:

$$\begin{aligned} \frac{\partial \boldsymbol{\sigma}_l(t, \mathbf{r})}{\partial t} = & \rho (c_{P,l}^2 - 2c_{S,l}^2) (\nabla \cdot \mathbf{v}_l(t, \mathbf{r})) \mathbf{I} + \\ & + \rho c_{S,l}^2 (\nabla \otimes \mathbf{v}_l(t, \mathbf{r}) + (\nabla \otimes \mathbf{v}_l(t, \mathbf{r}))^\top) - P(t, \mathbf{r}) \mathbf{I}, \end{aligned} \quad (1)$$

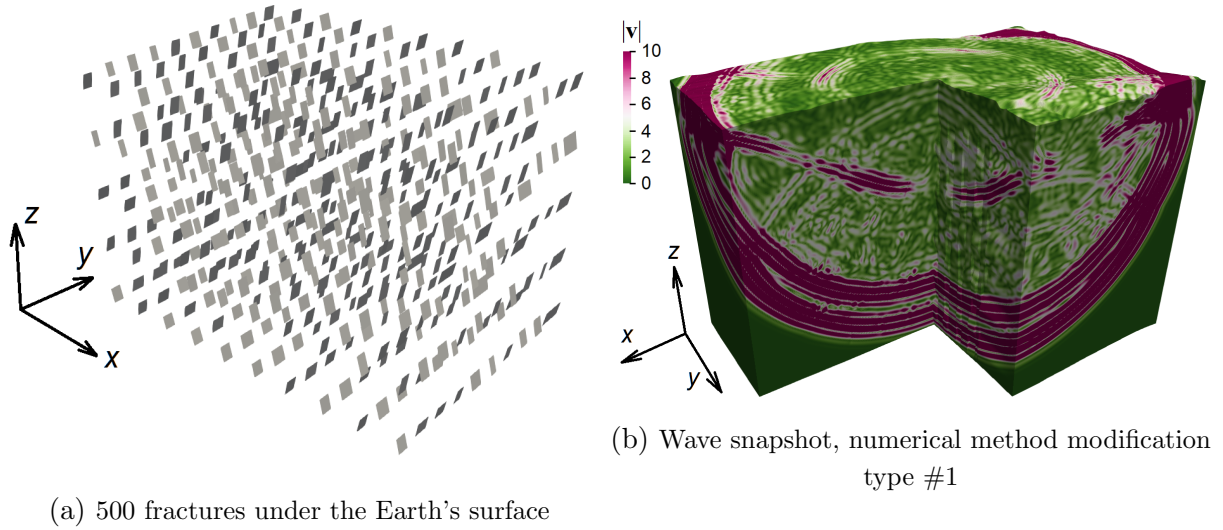


Figure 2. Example with 500 fractures in geological media

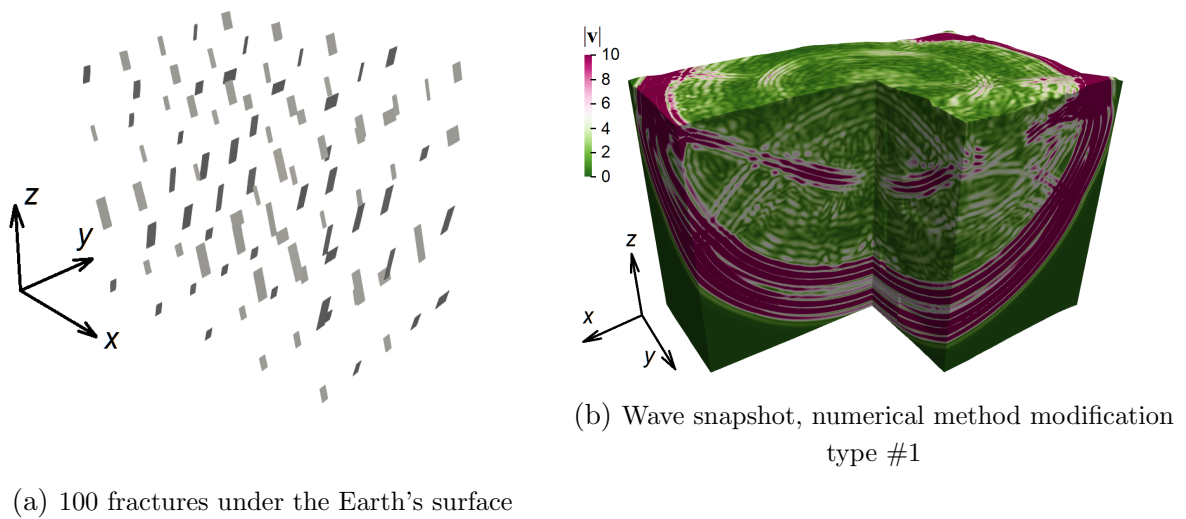


Figure 3. Example with 100 fractures in geological media

$$\rho_l \frac{\partial \mathbf{v}_l(t, \mathbf{r})}{\partial t} = (\nabla \cdot \boldsymbol{\sigma}_l(t, \mathbf{r}))^\top,$$

$$\mathbf{r} \in \Omega_l, t \in [0, T], l \in [1, L].$$

Here, in Eq. (1), the right-hand side (the seismic wave source) is described by the following expression:

$$P(t, \mathbf{r}) = \begin{cases} \left(1 - 2(\pi f t - 1.3\sqrt{6})^2\right) \exp\left(-(\pi f t - 1.3\sqrt{6})^2\right), & t \in \left[0, 3.9 \frac{\sqrt{6}}{\pi f}\right], \mathbf{r} \in \Xi, \\ 0, & t \notin \left[0, 3.9 \frac{\sqrt{6}}{\pi f}\right], \mathbf{r} \notin \Xi. \end{cases} \quad (2)$$

Here, in Eq. (2), the numerical coefficients arise in order to use the exact zero value on that part of the real time axis where the Ricker wavelet is sufficiently small.

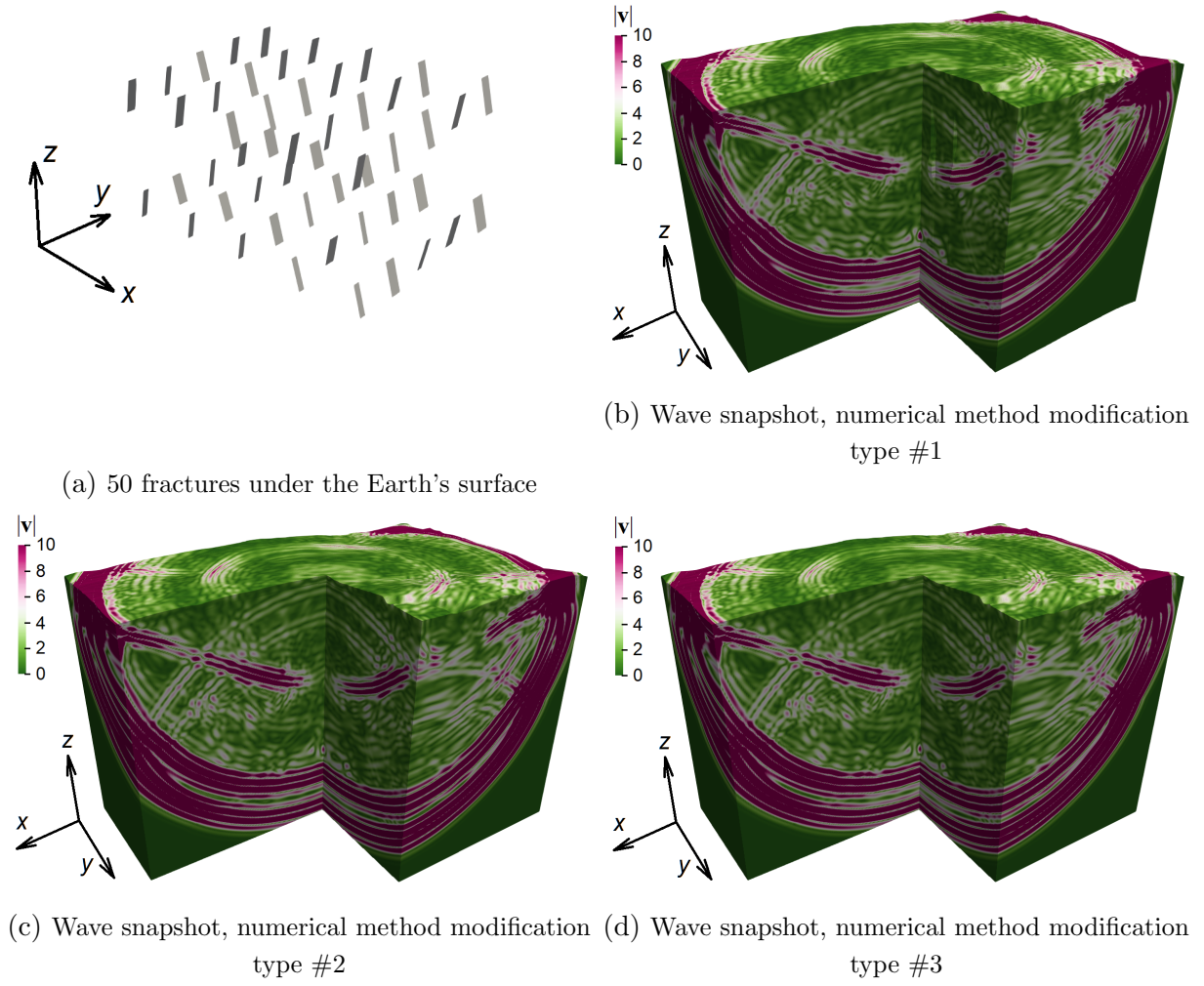


Figure 4. Example with 50 fractures in geological media

The following free boundary condition is established on the upper layer #1, at the contact with air:

$$\boldsymbol{\sigma}_1(t, \mathbf{r}) \cdot \mathbf{m}_1(\mathbf{r}) = 0,$$

$$\mathbf{m}_1(\mathbf{r}) \perp \Gamma_0, \mathbf{r} \in \Gamma_0, t \in [0, T].$$

At the boundaries of the sections of geological rocks, the following contact conditions are established:

$$\boldsymbol{\sigma}_{l-1}(t, \mathbf{r}) \cdot \mathbf{m}_l(\mathbf{r}) = \boldsymbol{\sigma}_l(t, \mathbf{r}) \cdot \mathbf{m}_l(\mathbf{r}),$$

$$\mathbf{v}_{l-1}(t, \mathbf{r}) = \mathbf{v}_l(t, \mathbf{r}),$$

$$\mathbf{m}_l(\mathbf{r}) \perp \Gamma_l, \mathbf{r} \in \Gamma_l, t \in [0, T], l \in [2, L].$$

The following contact condition is established, which is a special case [12] of Schoenberg linear slip model [19], to describe the scattering of waves on the fracture # i at the location of the fracture:

$$\mathbf{m}_i(\mathbf{r}) \cdot \boldsymbol{\sigma}_i^L(t, \mathbf{r}) \cdot \mathbf{m}_i(\mathbf{r}) = \mathbf{m}_i(\mathbf{r}) \cdot \boldsymbol{\sigma}_i^R(t, \mathbf{r}) \cdot \mathbf{m}_i(\mathbf{r}),$$

$$\boldsymbol{\sigma}_i^L(t, \mathbf{r}) \cdot \mathbf{m}_i(\mathbf{r}) - (\mathbf{m}_i(\mathbf{r}) \cdot \boldsymbol{\sigma}_i^L(t, \mathbf{r}) \cdot \mathbf{m}_i(\mathbf{r})) \mathbf{m}_i(\mathbf{r}) = 0,$$

$$\sigma_l^R(t, \mathbf{r}) \cdot \mathbf{m}_i(\mathbf{r}) - (\mathbf{m}_i(\mathbf{r}) \cdot \sigma_l^R(t, \mathbf{r}) \cdot \mathbf{m}_i(\mathbf{r})) \mathbf{m}_i(\mathbf{r}) = 0,$$

$$\mathbf{v}_l^L(t, \mathbf{r}) \cdot \mathbf{m}_i(\mathbf{r}) = \mathbf{v}_l^R(t, \mathbf{r}) \cdot \mathbf{m}_i(\mathbf{r}),$$

$$\mathbf{m}_i(\mathbf{r}) \perp \Theta_i, \mathbf{r} \in \Theta_i, t \in [0, T], i \in [1, F].$$

Here and further in the text, σ is Cauchy stress tensor, \mathbf{v} is velocity, c_P , c_S , and ρ are elastic parameters (P-wave speed, S-wave speed, and density), f means frequency, \mathbf{m} means unit normals, L is the number of geological layers, F is the number of fractures, Ξ is the source location, Γ_l is the boundary between l and $l + 1$ layers, Θ_i is the i fracture location.

2. Decomposition and Partitioning Algorithms

In this manuscript, we compare how the proposed decomposition algorithm works for three modifications of the grid-characteristic method, also varying the number of geological fractures. Examples of snapshots of wave fields are shown in Figs. 4b, 4c, and 4d for computational method modification types #1, #2, #3, respectively.

In calculations with numerical method modification type #1, we have the following set of computational grids:

- large computational grids, curvilinear structured grids covering geological layers in the amount of geological layers L , see Fig. 5a,
- tiny computational grids of the minimal size for identifying a rupture on a fracture in the amount of $2F$, see Fig. 6a.

That is, we have

$$G_L = L$$

large grids and

$$G_S = 2F$$

small grids.

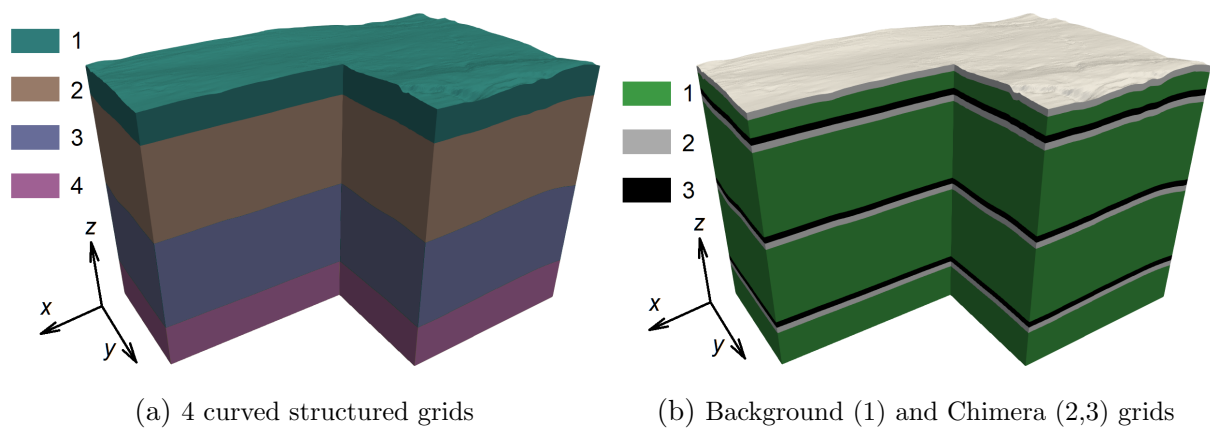
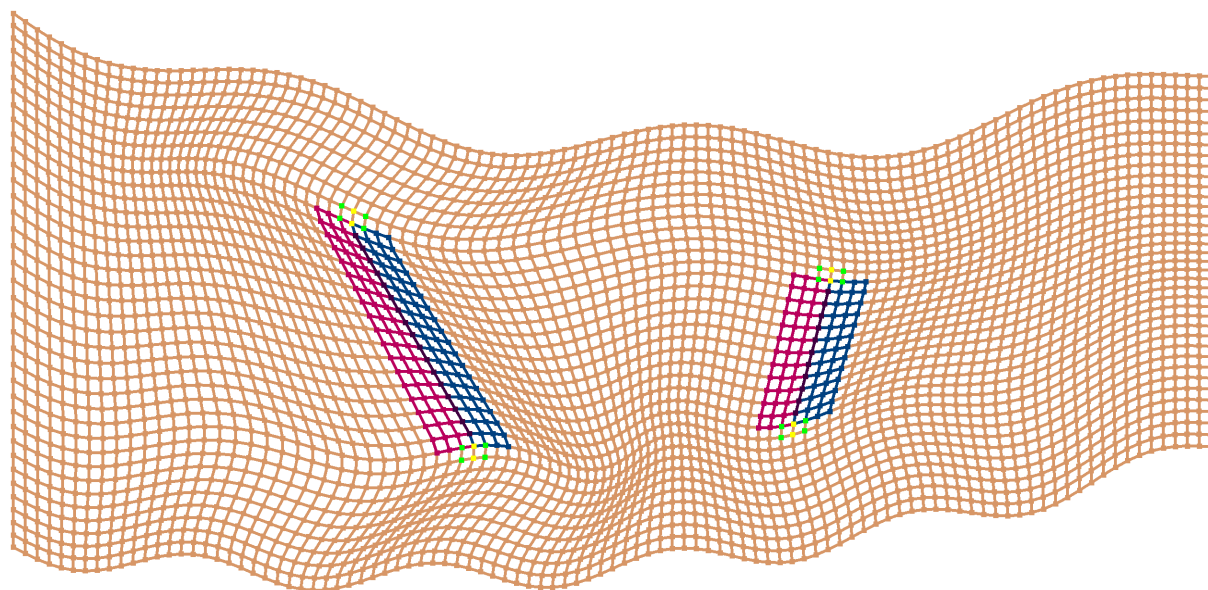
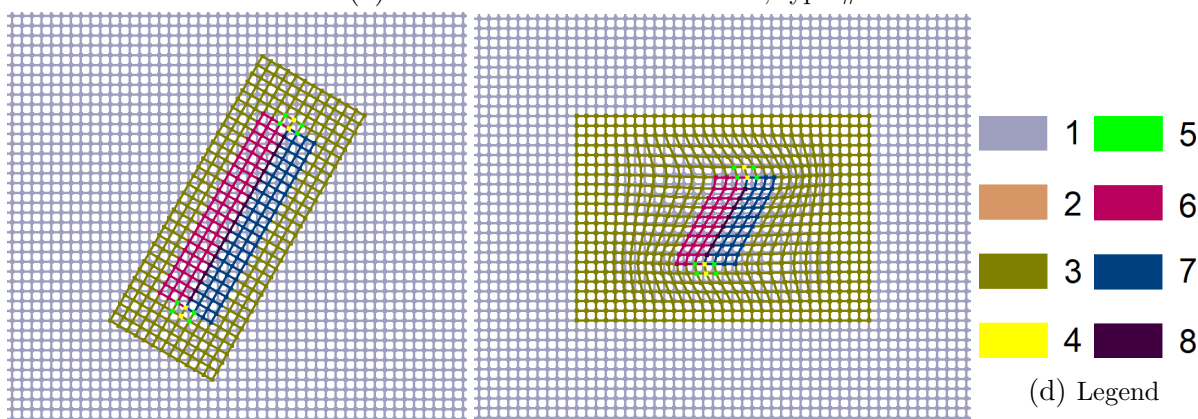


Figure 5. Large computational grids

At the legend in Fig. 6d, 1 is a part of large background Cartesian grid, 2 is a part of large curved structured grid covering geological layer, 3 is Chimera rotated Cartesian or curved structured patch grid around the fracture, 4 means nodes of grids of types 2 or 3, to which data is copied to smooth out the gap at the ends of the fracture, 5 means nodes of grids of types 2



(a) Numerical method modification, type #1



(b) Numerical method modification, type #2

(c) Numerical method modification, type #3

(d) Legend

Figure 6. Small and tiny computational grids around fractures, OXY, example

or 3, from which data is copied, 6 is left tiny grid of the minimal size around the fracture, 7 is right tiny grid of the minimal size around the fracture, 8 is the fracture itself.

In calculations with numerical method modifications types #2 and #3, we have the following set of computational grids:

- large Cartesian background grid, see Fig. 5b,
- large Chimera curvilinear computational grids along layers in the amount of $2L1$, see Fig. 5b,
- small computational grids around fractures in the amount of F (built according to different algorithms and having different number of nodes for calculations of type #2 (see Fig. 6b) and type #3 (see Fig. 6c), respectively),
- tiny computational grids of the minimal size for highlighting a rupture on a fracture in the amount of $2F$, see Figs. 6b and 6c for numerical method modifications types #2 and #3, respectively.

That is, we have

$$G_L = 8L$$

large grids and

$$G_S = 3F$$

small grids.

The number of computational operations spent on calculations on different types of grids is different. For example, we give below the formulae for calculating the first two Riemann invariants in the three-dimensional case for a Cartesian grid:

$$\omega_{1,2}^X = v_X \mp \frac{1}{\rho c_P} \sigma_{XX},$$

and for a curvilinear structured grid:

$$\omega_{1,2} = \mathbf{n} \cdot \mathbf{v} \mp \frac{1}{\rho c_P} (\mathbf{N}_{00} : \boldsymbol{\sigma}). \quad (3)$$

In Eq. (3), \mathbf{n} is a vector, and \mathbf{N}_{00} is a symmetric tensor of the second rank, depending on the node of the curved computational grid.

Therefore, before starting the calculations, the grid node weighting coefficients for each type of computational grid are determined by running test calculations, which do not take much time. The coefficients used in current study are given in Tab. 1.

Table 1. Weights of nodes in different types of computational grids

computational grid	figure	grid type	method type	weight w
grid covering geological layer	Fig. 5a	curved structured	#1	3.0
large background	Fig. 5b	Cartesian	#2, #3	1.0
large Chimera along interfaces	Fig. 5b	curved structured	#2, #3	2.0
small Chimera around fractures	Fig. 6b	Cartesian rotated	#2	1.0
small patch around fractures	Fig. 6c	curved structured	#3	4.0
tiny around fractures	Fig. 6a	curved structured	#1	2.0
tiny around fractures	Fig. 6b	Cartesian rotated	#2	1.0
tiny around fractures	Fig. 6c	curved structured	#3	2.0

We calculate the value

$$N = \sum_{g=1}^{G_L+G_S} w_g N_X^g N_Y^g N_Z^g$$

to perform the decomposition.

The numbers of processes allocated to the large grids are calculated using the following formulae:

$$P_g = \frac{P}{S} w_g N_X^g N_Y^g N_Z^g,$$

$$g \in [1, G_1].$$

Then these real numbers are rounded to an integers and the set of these numbers for all large grids is adjusted so that the sum does not exceed the total number of processes P :

$$P_F = P - \sum_{g=1}^{G_L} P_g,$$

$$P_F \geq 0.$$

Minimal Cross Section algorithm for parallel grid partitioning introduced in [3] is used for these large grids to divide each g grid by a selected number of processes P_g , $g \in [1, G_1]$.

1. All possible partitions of the number of processes P_g into 3 divisors $\{L_X^{g,j}, L_Y^{g,j}, L_Z^{g,j}\}$ are considered, without repetitions based on the known tables of natural numbers divisors. If the P_g has a large amount of divisors, one can choose not all divisors, but only some, approximately equidistant from each other, and including 1 and P_g .

$$P_g = L_X^{j,g} \cdot L_Y^{j,g} \cdot L_Z^{j,g}.$$

2. The sum of the cross sections is calculated for each set of divisors $\{L_X^{g,j}, L_Y^{g,j}, L_Z^{g,j}\}$ using the following formula:

$$S_g^j = \left(L_X^{g,j} - 1\right) \cdot N_Y^g \cdot N_Z^g + \left(L_Y^{g,j} - 1\right) \cdot N_X^g \cdot N_Z^g + \left(L_Z^{g,j} - 1\right) \cdot N_X^g \cdot N_Y^g.$$

3. Such a set of divisors $\{L_X^{g,j}, L_Y^{g,j}, L_Z^{g,j}\}$ is chosen, which provides the minimal value of the cross section S_g^j .

Then the distribution of small (and tiny) grids among the processes begins.

In the case of a modification of the numerical method of type #1, at first the P_F processes are filled with the number of grids sequentially each, until the total number of nodes allocated to the process begins to exceed the average filling of the remaining processes with nodes of large grids $\frac{N}{P}$. In this case and further, the nodes are taken into account with weights. That is, the value $w_g N_X^g N_Y^g N_Z^g$ is considered, and not $N_X^g N_Y^g N_Z^g$. The remaining part of the tiny grids of the minimal size is distributed evenly among all processes evenly.

For modifications of the numerical method of types #2, #3, the coefficient of the ratio K of the average size of the small grid around the fracture to the average size of the tiny grid of the minimal size is calculated. Then,

1. The P_F processes are filled according to the following algorithm sequentially each.
 - (a) We try to place as many small grids around the fractures as possible so that the total number of nodes in the process under consideration does not exceed $\frac{N}{P}$.
 - (b) If possible, we place as many tiny grids of the minimal size as possible.
 - (c) We move on to the next process.
2. We distribute the remaining small grids around the fractures evenly across all processes until we stop at process number P_0 .
3. We place K tiny grids of minimal size into the remaining PP_0 processes.
4. We distribute the remaining tiny grids of minimal size evenly across all processes evenly.

Note that, the P_F number is often zero for an insufficiently large number of fractures and number of MPI processes, see Tables 2–4.

As for large Chimera grids placed along geological layers, for a small number of MPI processes, one process also often has been allocated for each large Chimera grid, see Tables 5 and 6.

Table 2. Dependence of the number of MPI processes allocated to all grids around fractures only P_F on the total number of MPI processes P for the different number of fractures, numerical method modification type #1

P	12	16	20	24	28	32	40	50	60	70	80	90	100	150	250	500
50	1	0	0	1	0	0	1	1	0	0	1	0	0	1	1	2
100	1	0	0	1	1	0	1	1	0	0	1	0	0	1	1	2
500	1	1	0	1	1	1	2	1	1	2	3	2	2	4	6	13
1000	1	1	2	1	1	1	2	2	4	4	4	4	5	8	13	24
2000	1	1	2	2	2	3	3	5	5	6	7	9	10	13	23	47

Table 3. Dependence of the number of MPI processes allocated to all grids around fractures only P_F on the total number of MPI processes P for the different number of fractures, numerical method modification type #2

P	12	16	20	24	28	32	40	50	60	70	80	90	100	150	250	500
50	0	0	2	0	0	1	0	2	0	0	2	0	0	0	3	0
100	0	0	2	0	0	1	0	2	0	0	2	0	4	0	3	7
500	0	1	3	0	0	1	0	3	1	5	3	1	6	9	8	22
1000	0	1	3	5	0	2	6	4	2	7	5	10	8	12	19	39
2000	0	2	4	6	1	3	7	6	11	9	8	13	11	24	35	70

Table 4. Dependence of the number of MPI processes allocated to all grids around fractures only P_F on the total number of MPI processes P for the different number of fractures, numerical method modification type #3

P	12	16	20	24	28	32	40	50	60	70	80	90	100	150	250	500
50	0	0	2	0	0	1	0	2	0	0	2	0	4	0	4	8
100	0	1	2	0	0	1	0	3	0	5	3	0	5	1	6	11
500	0	1	3	5	1	3	7	5	10	8	6	12	10	15	25	56
1000	0	2	4	7	9	4	9	7	13	12	17	16	22	29	51	101
2000	1	3	6	8	11	13	12	18	17	24	30	30	36	47	83	165

Therefore, the decomposition algorithm proposed in this manuscript is not suitable for a small number of MPI processes.

Table 5. Dependence of the number of MPI processes allocated to one large Chimera grid on the total number of MPI processes P for the different number of fractures, numerical method modification type #2

P	12	16	20	24	28	32	40	50	60	70	80	90	100	150	250	500
50	1	1	1	1	1	2	2	3	4	4	5	6	6	9	16	32
100	1	1	1	1	1	2	2	3	4	4	5	6	6	9	16	32
500	1	1	1	1	2	2	2	3	4	4	5	6	6	9	16	31
1000	1	1	1	1	2	2	2	3	4	4	5	5	6	9	15	30
2000	1	1	1	1	2	2	2	3	3	4	5	5	6	8	14	28

Table 6. Dependence of the number of MPI processes allocated to one large Chimera grid on the total number of MPI processes P for the different number of fractures, numerical method modification type #3

P	12	16	20	24	28	32	40	50	60	70	80	90	100	150	250	500
50	1	1	1	1	1	2	2	3	4	4	5	6	6	10	16	32
100	1	1	1	1	1	2	2	3	4	4	5	6	6	10	16	32
500	1	1	1	1	2	2	2	3	3	4	5	5	6	9	15	29
1000	1	1	1	1	1	2	2	3	3	4	4	5	5	8	13	26
2000	1	1	1	1	1	1	2	2	3	3	3	4	4	7	11	22

3. Speed Up Testing

This section presents the graphs of the speedup dependence on the number of MPI processes for various modifications of the numerical method and various numbers of fractures in Fig. 7.

The 9 dependences of the speedup on the number of MPI processes are grouped on the graphs as follows. For the same types of numerical method modification and different numbers of fractures on one graph in Figs. 7a, 7c, and 7e for types #1, #2, #3, respectively. For the same numbers of fractures and different numerical methods modifications on the same graph in Figs. 7b, 7d, and 7f for the numbers of fractures 50, 100, 500, respectively.

Thus, Figs. 7a, 7c, and 7e allow one to see the effect of the number of fractures on the parallelization efficiency. While Figs. 7b, 7d, and 7f allow one to compare the parallelization efficiency of different modifications of the numerical method for the same number of fractures.

Conclusion

In the manuscript, we proposed and studied the algorithm for decomposing a large number of individual computational grids of various sizes using the example of a direct problem of seismic exploration of geological media treating the complex topology of the Earth’s surface, the complex shape of interfaces between geological layers, and a large number of explicitly treated geological fractures, that are not aligned with the coordinate axes. The developed decomposition algorithm was tested for three modifications of the grid-characteristic method on Chimera and curvilinear structured computational grids. The effect of the number of fractures on the efficiency of parallelization was studied.

The modification of the numerical method type #1 is more efficiently parallelized. But, when this modification is applied, the complexity is the construction of curvilinear structured grids, which, on the one hand, allow describing the complex topography of interfaces between geological rocks and the Earth’s surface boundary-conforming, and on the other hand, node by node, geometrically fall into each fracture. Such computational grids are difficult to construct with a large number of geological fractures, both algorithmically and in terms of RAM and time costs at the preprocessing stage.

The modification of the numerical method type #3 is more accurate computationally (see works [12, 13]), but loses in parallelization efficiency in comparison to type #2 with a large number of fractures and a large number of MPI processes and large fracture inclination angles relative to the coordinate axes. This is due to the fact that the modification of the method type

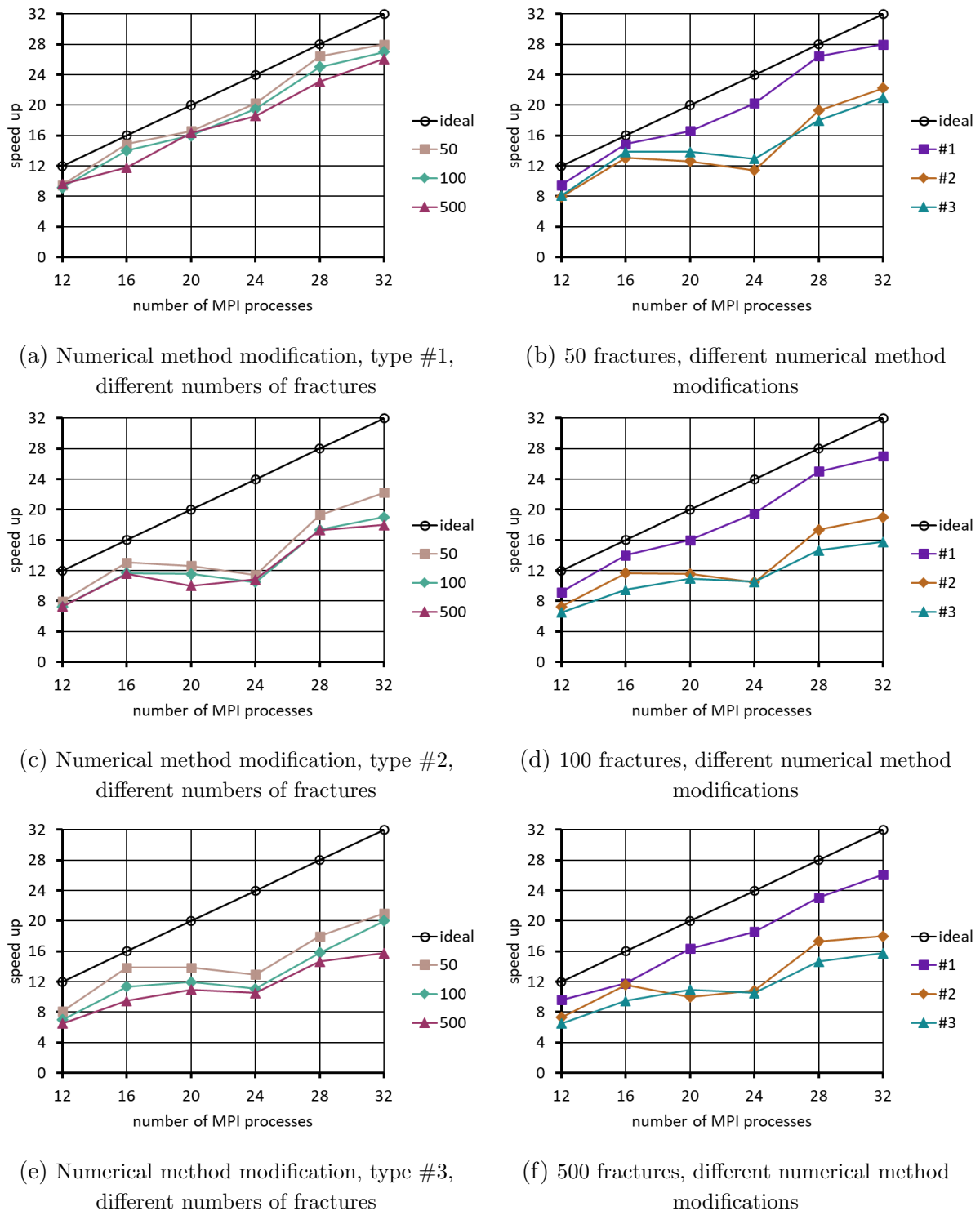


Figure 7. Dependences of the speedup on the number of MPI processes

#3 requires constructing a grid around a fracture of a slightly larger size (see Figs. 6b and 6c) compared to type #2, and this begins to affect under the above conditions.

For all modifications of the numerical method, the growth of fracture number leads to an increase in the volume of transmitted information, which reduces the efficiency of parallelization. The effect is weakest for the modification of the numerical method type #1, since this modification contains only tiny computational grids of minimal size around fractures. In turn,

for the modification of the numerical method type #3, the effect is somewhat stronger than for the modification of the numerical method type #2 for the same reason.

As a direction for further development of the proposed in the manuscript decomposition algorithm, we can name the identification of the dependence of weight coefficients for grids around fractures taking into account the average amount of transmitted data.

Acknowledgements

The research was supported by the Russian Science Foundation grant No. 20-71-10028, <https://rscf.ru/project/20-71-10028/>. This work has been carried out using computing resources of the federal collective usage center Complex for Simulation and Data Processing for Mega-science Facilities at NRC “Kurchatov Institute”, <http://ckp.nrcki.ru/>.

This paper is distributed under the terms of the Creative Commons Attribution-Non Commercial 3.0 License which permits non-commercial use, reproduction and distribution of the work without further permission provided the original work is properly cited.

References

1. Badia, S., Martín, A.F., Principe, J.: A highly scalable parallel implementation of balancing domain decomposition by constraints. *SIAM Journal on Scientific Computing* 36(2), C190–C218 (2014), <https://doi.org/10.1007/s11075-022-01268-0>
2. Favorskaya, A., Khokhlov, N.: Accounting for curved boundaries in rocks by using curvilinear and Chimera grids. *Procedia Computer Science* 192, 3787–3794 (2021), <https://doi.org/10.1016/j.procs.2021.09.153>
3. Favorskaya, A., Khokhlov, N., Sagan, V., Podlesnykh, D.: Parallel computations by the grid-characteristic method on Chimera computational grids in 3D problems of railway non-destructive testing. In: Voevodin, V., Sobolev, S., Yakobovskiy, M., Shagaliev, R. (eds.) *Supercomputing. RuSCDays 2022, Lecture Notes in Computer Science*, vol. 13708, pp. 199–213. Springer, Cham (2022), https://doi.org/10.1007/978-3-031-22941-1_14
4. Favorskaya, A., Petrov, I., Grinevskiy, A.: Numerical simulation of fracturing in geological medium. *Procedia Computer Science* 112, 1216–1224 (2017), <https://doi.org/10.1016/j.procs.2017.08.042>
5. Favorskaya, A.V., Khokhlov, N.I., Petrov, I.B.: Grid-characteristic method on joint structured regular and curved grids for modeling coupled elastic and acoustic wave phenomena in objects of complex shape. *Lobachevskii Journal of Mathematics* 41, 512–525 (2020), <https://doi.org/10.1134/S1995080220040083>
6. Favorskaya, A.V., Petrov, I.B.: The use of full-wave numerical simulation for the investigation of fractured zones. *Mathematical Models and Computer Simulations* 11, 518–530 (2019), <https://doi.org/10.1134/S2070048219040069>
7. Golubev, V., Nikitin, I., Beklemysheva, K.: Model of fractured medium and nondestructive control of composite materials. *Chinese Journal of Aeronautics* 37(2), 93–99 (2024), <https://doi.org/10.1016/j.cja.2023.11.023>

8. Golubev, V., Nikitin, I., Vasyukov, A., Nikitin, A.: Fractured inclusion localization and characterization based on deep convolutional neural networks. *Procedia Structural Integrity* 43, 29–34 (2023), <https://doi.org/10.1016/j.prostr.2022.12.230>
9. Goncharsky, A.V., Romanov, S.Y., Seryozhnikov, S.Y.: Supercomputer technologies in tomographic imaging applications. *Supercomputing Frontiers and Innovations* 3(1), 41–66 (2016), <https://doi.org/10.14529/jsfi160103>
10. Hall, F., Wang, Y.: Seismic response of fractures by numerical simulation. *Geophysical Journal International* 189(1), 591–601 (2012), <https://doi.org/10.1111/j.1365-246X.2012.05360.x>
11. Henshaw, W.D., Schwendeman, D.W.: Parallel computation of three-dimensional flows using overlapping grids with adaptive mesh refinement. *Journal of Computational Physics* 227(16), 7469–7502 (2008), <https://doi.org/10.1016/j.jcp.2008.04.033>
12. Khokhlov, N., Favorskaya, A., Stetsyuk, V., Mitskovets, I.: Grid-characteristic method using Chimera meshes for simulation of elastic waves scattering on geological fractured zones. *Journal of Computational Physics* 446, 110637 (2021), <https://doi.org/10.1016/j.jcp.2021.110637>
13. Khokhlov, N.I., Favorskaya, A.V., Furgailo, V.: Grid-characteristic method on overlapping curvilinear meshes for modeling elastic waves scattering on geological fractures. *Minerals* 12(12), 1597 (2022), <https://doi.org/10.3390/min12121597>
14. Micucci, M., Iula, A.: Recent advances in machine learning applied to ultrasound imaging. *Electronics* 11(11), 1800 (2022), <https://doi.org/10.3390/electronics11111800>
15. Muratov, M., Ryazanov, V., Biryukov, V., Petrov, D., Petrov, I.: Inverse problems of heterogeneous geological layers exploration seismology solution by methods of machine learning. *Lobachevskii Journal of Mathematics* 42(7), 1728–1737 (2021), <https://doi.org/10.1134/S1995080221070180>
16. Pleshkevich, A.L., Ivanov, A.V., Levchenko, V.D., *et al.*: Efficient parallel implementation of multi-arrival 3D prestack seismic depth migration. *Supercomputing Frontiers and Innovations* 6(1), 4–8 (2019), <https://doi.org/10.14529/jsfi190101>
17. Qi, Y., Chen, X., Zhao, Q., *et al.*: Seismic wave modeling of fluid-saturated fractured porous rock: including fluid pressure diffusion effects of discretely distributed large-scale fractures. *Solid Earth* 15(4), 535–554 (2024), <https://doi.org/10.5194/se-15-535-2024>
18. Rybakin, B., Goryachev, V.: Heterogeneous computing systems in problems of modeling filaments formation and pre-stellar objects. In: Voevodin, V., Sobolev, S., Yakobovskiy, M., Shagaliev, R. (eds.) *Supercomputing. RuSCDays 2022, Lecture Notes in Computer Science*, vol. 13708, pp. 127–139. Springer, Cham (2022), https://doi.org/10.1007/978-3-031-22941-1_9
19. Schoenberg, M.: Elastic wave behavior across linear slip interfaces. *The Journal of the Acoustical Society of America* 68(5), 1516–1521 (1980), <https://doi.org/10.1121/1.385077>

20. Vamaraju, J., Sen, M.K., De Basabe, J., Wheeler, M.: A hybrid Galerkin finite element method for seismic wave propagation in fractured media. *Geophysical Journal International* 221(2), 857–878 (2020), <https://doi.org/10.1093/gji/ggaa037>
21. Wang, K., Peng, S., Lu, Y., Cui, X.: The velocity-stress finite-difference method with a rotated staggered grid applied to seismic wave propagation in a fractured medium. *Geophysics* 85(2), T89–T100 (2020), <https://doi.org/10.1190/geo2019-0186.1>
22. Xiang, Y., Wang, Z., Song, Z., *et al.*: Seismictransformer: An attention-based deep learning method for the simulation of seismic wavefields. *Computers & Geosciences* p. 105629 (2024), <https://doi.org/10.1016/j.cageo.2024.105629>
23. Xu, J., Hu, H., Liu, Q.H., Zhan, Q., Zhuang, M.: Spectral element modeling of elastic wave propagation in an anisotropic background with discrete anisotropic fractures. *Geophysical Journal International* 227(2), 832–848 (2021), <https://doi.org/10.1093/gji/ggab226>
24. Xu, Y., Chen, X., Zhang, W., Pan, X.: An adaptive modal discontinuous Galerkin finite element parallel method using unsplit multi-axial perfectly matched layer for seismic wave modeling. *Commun. Comput. Phys.* 31(4), 1083–1113 (2022). <https://doi.org/10.4208/cicp.0A-2021-0118>